remote sensing

MDPI

Article

Discrimination of Degraded Pastures in the Brazilian Cerrado Using the PlanetScope SuperDove Satellite Constellation

Angela Gabrielly Pires Silva [1], Lênio Soares Galvão [1,*], Laerte Guimarães Ferreira Júnior [2], Nathália Monteiro Teles [2], Vinícius Vieira Mesquita [2] and Isadora Haddad [1]

[1] Divisão de Observação da Terra e Geoinformática (DIOTG), Instituto Nacional de Pesquisas Espaciais (INPE), São José dos Campos 12245-970, SP, Brazil; angela.pires@inpe.br (A.G.P.S.); isadora.ruiz@inpe.br (I.H.)
[2] Laboratório de Processamento de Imagens e Geoprocessamento (LAPIG), Universidade Federal de Goiás—UFG, Campus II, LAPIG, Goiânia 74001-970, GO, Brazil; laerte@ufg.br (L.G.F.J.); nathalia.teles@ufg.br (N.M.T.); vieiramesquita@gmail.com (V.V.M.)
* Correspondence: lenio.galvao@inpe.br

Abstract: Pasture degradation poses significant economic, social, and environmental impacts in the Brazilian savanna ecosystem. Despite these impacts, effectively detecting varying intensities of agronomic and biological degradation through remote sensing remains challenging. This study explores the potential of the eight-band PlanetScope SuperDove satellite constellation to discriminate between five classes of pasture degradation: non-degraded pasture (NDP); pastures with low- (LID) and moderate-intensity degradation (MID); severe agronomic degradation (SAD); and severe biological degradation (SBD). Using a set of 259 cloud-free images acquired in 2022 across five sites located in central Brazil, the study aims to: (i) identify the most suitable period for discriminating between various degradation classes; (ii) evaluate the Random Forest (RF) classification performance of different SuperDove attributes; and (iii) compare metrics of accuracy derived from two predicted scenarios of pasture degradation: a more challenging one involving five classes (NDP, LID, MID, SAD, and SBD), and another considering only non-degraded and severely degraded pastures (NDP, SAD, and SBD). The study assessed individual and combined sets of SuperDove attributes, including band reflectance, vegetation indices, endmember fractions from spectral mixture analysis (SMA), and image texture variables from Gray-level Co-occurrence Matrix (GLCM). The results highlighted the effectiveness of the transition from the rainy to the dry season and the period towards the beginning of a new seasonal rainy cycle in October for discriminating pasture degradation. In comparison to the dry season, more favorable discrimination scenarios were observed during the rainy season. In the dry season, increased amounts of non-photosynthetic vegetation (NPV) complicate the differentiation between NDP and SBD, which is characterized by high soil exposure. Pastures exhibiting severe biological degradation showed greater sensitivity to water stress, manifesting earlier reflectance changes in the visible and near-infrared bands of SuperDove compared to other classes. Reflectance-based classification yielded higher overall accuracy (OA) than the approaches using endmember fractions, vegetation indices, or texture metrics. Classifications using combined attributes achieved an OA of 0.69 and 0.88 for the five-class and three-class scenarios, respectively. In the five-class scenario, the highest F1-scores were observed for NDP (0.61) and classes of agronomic (0.71) and biological (0.88) degradation, indicating the challenges in separating low and moderate stages of pasture degradation. An initial comparison of RF classification results for the five categories of degraded pastures, utilizing reflectance data from MultiSpectral Instrument (MSI)/Sentinel-2 (400–2500 nm) and SuperDove (400–900 nm), demonstrated an enhanced OA (0.79 versus 0.66) with Sentinel-2 data. This enhancement is likely to be attributed to the inclusion of shortwave infrared (SWIR) spectral bands in the data analysis. Our findings highlight the potential of satellite constellation data, acquired at high spatial resolution, for remote identification of pasture degradation.

Keywords: pasture degradation; savanna; spectral mixture; vegetation indices; random forest

check for updates

Citation: Silva, A.G.P.; Galvão, L.S.; Ferreira Júnior, L.G.; Teles, N.M.; Mesquita, V.V.; Haddad, I. Discrimination of Degraded Pastures in the Brazilian Cerrado Using the PlanetScope SuperDove Satellite Constellation. *Remote Sens.* **2024**, *16*, 2256. https://doi.org/10.3390/rs16132256

Academic Editor: Clement Atzberger

Received: 30 April 2024
Revised: 17 June 2024
Accepted: 19 June 2024
Published: 21 June 2024

Copyright: © 2024 by the authors. Licensee MDPI, Basel, Switzerland. This article is an open access article distributed under the terms and conditions of the Creative Commons Attribution (CC BY) license (https://creativecommons.org/licenses/by/4.0/).

1. Introduction

Despite being the world's largest meat exporter, Brazil primarily practices extensive livestock farming. Pasturelands, occupying approximately 21% of the national territory, are predominantly found in the central savanna environment known as the Cerrado biome [1]. Cultivated and natural pastures cover around 180 million hectares of Brazilian land, with 35% of this area situated in the Cerrado [2]. Satellite imagery from 2018 suggests that about 59% of Brazilian pasturelands experienced some level of degradation [3].

The term "pasture degradation" refers to the gradual decline in vigor, productivity, and natural regeneration capacity of a specific pasture [4]. As this process unfolds, the pasture becomes incapable of sustaining the necessary levels of production and quality required by the animals. Additionally, it loses resilience and resistance to the adverse impacts of pests, diseases, and invasive plants. Degradation is commonly linked to inadequate animal stocking practices, insufficient pest control, presence of invasive plants, and lack of fertilization [5].

Given the substantial economic, social, and environmental impacts associated with pasture degradation, there is a significant interest in accurately mapping degraded areas in Brazil. This interest is fueled by the recognition that well-managed and productive pasturelands have the potential to enhance carbon sequestration and reduce carbon emissions [6–8]. Another compelling reason for mapping these areas is to devise strategies or policies aimed at the potential conversion of degraded pastures into reforested areas or agricultural land [8,9]. For example, through effective management of degraded pastures, these areas can be transformed into soybean fields, contributing to increased crop production without causing deforestation or clearing of native vegetation in both the Cerrado and Amazon biomes.

Traditionally, the assessment of pasture degradation involves extensive fieldwork sampling and labor-intensive laboratory analyses, rendering this method both costly and time-consuming. This is particularly challenging for systematically monitoring vast areas in Brazil, one of the world's largest countries. Realistically, remote sensing emerges as the most suitable approach for systematically covering pasturelands in a short timeframe and providing rapid assessments of their quality with adequate support of field information. Nevertheless, employing remote sensing to discriminate classes of pasture degradation poses challenges in Brazil, particularly in the Cerrado, due to subtle differences in reflectance between degraded and non-degraded sites. Therefore, there is an ongoing need to explore and test various remote sensing approaches and datasets for the systematic mapping of pasture degradation in the Cerrado biome [3].

Most remote sensing investigations on pasture degradation in Brazil have predominantly used data obtained with low-to-moderate (250 to 1000 m) or medium (30 m) spatial resolution, derived from instruments such as the Moderate Resolution Imaging Spectroradiometer (MODIS)/Terra or satellites such as the Landsat [10–14]. Various analytical approaches have been employed worldwide to map pastures using these data with advantages and disadvantages. Such approaches involve, for instance, time series analysis of MODIS vegetation indices [11,15–17]. However, certain degraded pastures, dominated by invasive plant species or weeds, may, in fact, exhibit an increase in vegetation indices over time when observed by satellites, contrary to the anticipated long-term decline expected for degraded areas. Other methodologies for mapping pasture degradation encompass the use of classification techniques applied to Landsat [18–21], Synthetic Aperture Radar (SAR) [22], or hyperspectral data [23–25].

In reality, various classes of pasture degradation are often overlooked in most studies, including low-intensity degradation (LID), moderate-intensity degradation (MID), severe agronomic degradation (SAD), and severe biological degradation (SBD). Mapping these distinct classes in the Cerrado environment, along with non-degraded pastures (NDP), proves to be crucial yet challenging when employing remote sensing techniques. Detailed mapping of degraded pastures is vital for understanding their nuanced impacts, influencing the costs associated with their recovery, and defining strategies necessary for restoration.

Regrettably, existing literature lacks comprehensive studies testing the discrimination of different levels of pasture degradation and examining how these areas respond spectrally and seasonally to the satellites. The precise identification of pastures at various stages of degradation becomes instrumental in supporting public policies aimed at their renewal or recovery, catering to both livestock intensification and the generation of surplus low-cost open land for alternative uses [26].

In this context, the recent introduction of the PlanetScope satellite constellation by Planet Labs PBC. holds significant promise for distinguishing non-degraded pastures from areas exhibiting varying levels of degradation. The third generation of CubeSats, known as SuperDove, has been consistently capturing daily data since 2020, utilizing eight spectral bands positioned between 400 and 900 nm (including blue I and II, green I and II, red I and II, red-edge, and near-infrared (NIR)). Offering a spatial resolution of 3.7 m and a radiometric resolution of 12 bits, SuperDove's dense time series of observations have the potential to reveal nuanced differences in reflectance corresponding to the condition and degradation stage of pastures. Despite this considerable potential, the application of SuperDove data in studies of pasture degradation in Brazil remains unexplored.

To address the complexity of spectral discrimination among various levels of pasture degradation, diverse metrics can be extracted from SuperDove data and subsequently subjected to machine learning classification. Among the various classification techniques employed for mapping savannas in Brazil, Random Forest (RF) has consistently demonstrated adequate performance compared to other classifiers [27–30]. Even when compared with deep learning approaches, RF has showed slightly lower F1-scores, as demonstrated with validation data by Parente et al. [31] in a study to separate pasture from non-pasture areas in the Cerrado. Therefore, RF is a suitable technique for handling a large number of metrics, as it operates as an ensemble of decision trees, with the final classification being determined by the most voted class [32,33].

Examples of metrics that can be used as input data for RF classification include the reflectance values from the eight bands of SuperDove, a suite of derived vegetation indices, endmember fractions obtained through Spectral Mixture Analysis (SMA), and image texture attributes. Using the SuperDove data, the suite of derived vegetation indices encompasses the Enhanced Vegetation Index (EVI) [34], the Green-Red Normalized Difference (GRND) [35], the Modified Photochemical Reflectance Index (MPRI) as a variant of the original formulation [36], the Normalized Difference Vegetation Index (NDVI) [37], and the Red-Edge Normalized Difference (REND) [38]. Some of these vegetation indices are sensitive to vegetation structure, while others can effectively monitor changes in new foliage and pigments within pastures [39].

Considering the significance of soil cover in assessing degradation in the field [40], approaches utilizing SMA can become valuable. Particularly, data associated with endmember-soil fractions in areas marked by severe biological degradation (SBD) with comparatively high soil exposure can be instrumental. These endmember fractions can, therefore, be considered as input data for a given classification model. The same principle holds for image texture metrics calculated from the Gray-Level Co-occurrence Matrix (GLCM). Changes in the relative proportions of soil and green vegetation, induced by severe agronomic factors (e.g., invasive species) and biological degradation (e.g., soil exposure), can manifest as alterations in the heterogeneity of pasture surfaces.

In this context, the objective of the current work is to explore the potential of satellite constellation data for discriminating various levels of pasture degradation (NDP, LID, MID, SAD, and SBD) in the Brazilian Cerrado. To achieve this objective, attributes extracted from the eight-band SuperDove instrument, measured through 2022, were utilized for RF classification of both degraded and non-degraded pastures. In the data analysis, a comprehensive dataset comprising field and remote sensing data collected across five sites, each spanning 15 × 15 km, was employed to ensure the accurate representation of distinct pasture degradation classes.

More specifically, the objectives are to: (i) identify the most favorable period for discriminating these classes using 259 cloud-free images acquired across all sites through 2022; (ii) assess the performance of both individual and combined sets of SuperDove attributes, including reflectance, vegetation indices, endmember fractions, and GLCM texture metrics, during the previously selected period for RF classification of the pasture degradation classes; and (iii) compare the RF classification outcomes using the combined set of attributes in two discrimination scenarios: a more challenging one involving five classes (NDP, LID, MID, SAD, and SBD), and another considering only non-degraded and severely degraded pastures (NDP, SAD, and SBD). Preliminary analysis of MultiSpectral Instrument (MSI)/Sentinel-2 data is also considered here for comparison with SuperDove results.

2. Methodology

The essential steps, methodological procedures, and utilized data are presented in the flowchart of Figure 1, which are detailed below.

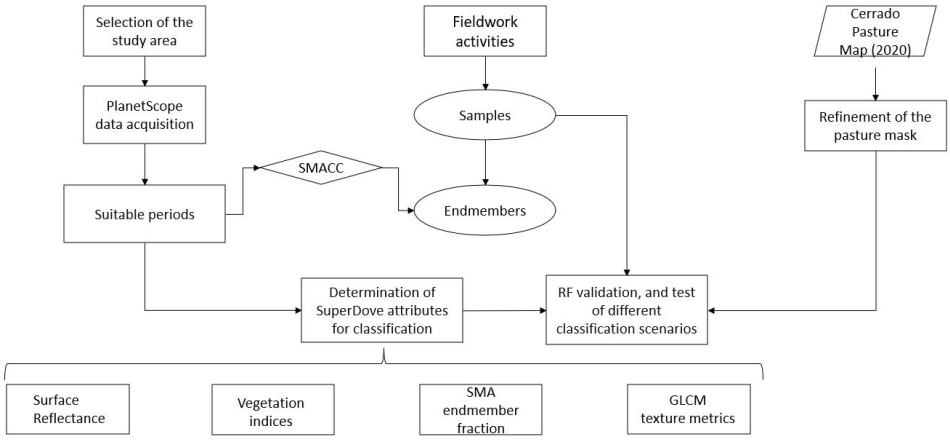


Figure 1. Summary of the methodology used in the current work to discriminate pasture degradation with SuperDove satellite constellation data.

2.1. Selection of the Study Area

The research focuses on the southeastern region of the Brazilian state of Goiás, characterized by climatic homogeneity in terms of precipitation. Within this region, five specific sites, each spanning 15 × 15 km in size, were chosen for the sampling of pastures exhibiting varying degrees of degradation (Figure 2). As per the Atlas of Pastures [41], the state of Goiás encompasses approximately 14 million hectares of pastures, with the selected study sites accounting for around 53,000 hectares.

In this savanna environment, the dry season (May to September) is marked by very low precipitation values (Figure 2). In the rainy season (October to April), rainfall is mostly concentrated between December and March. In contrast to the 20-year long-term average (2001–2021), the year 2022, during which the SuperDove images were captured, experienced reduced monthly precipitation levels at the studied sites. This discrepancy was particularly pronounced during the rainy season, notably in March and April. Meteorological station measurements at the five designated sites or municipalities corroborated this observation.

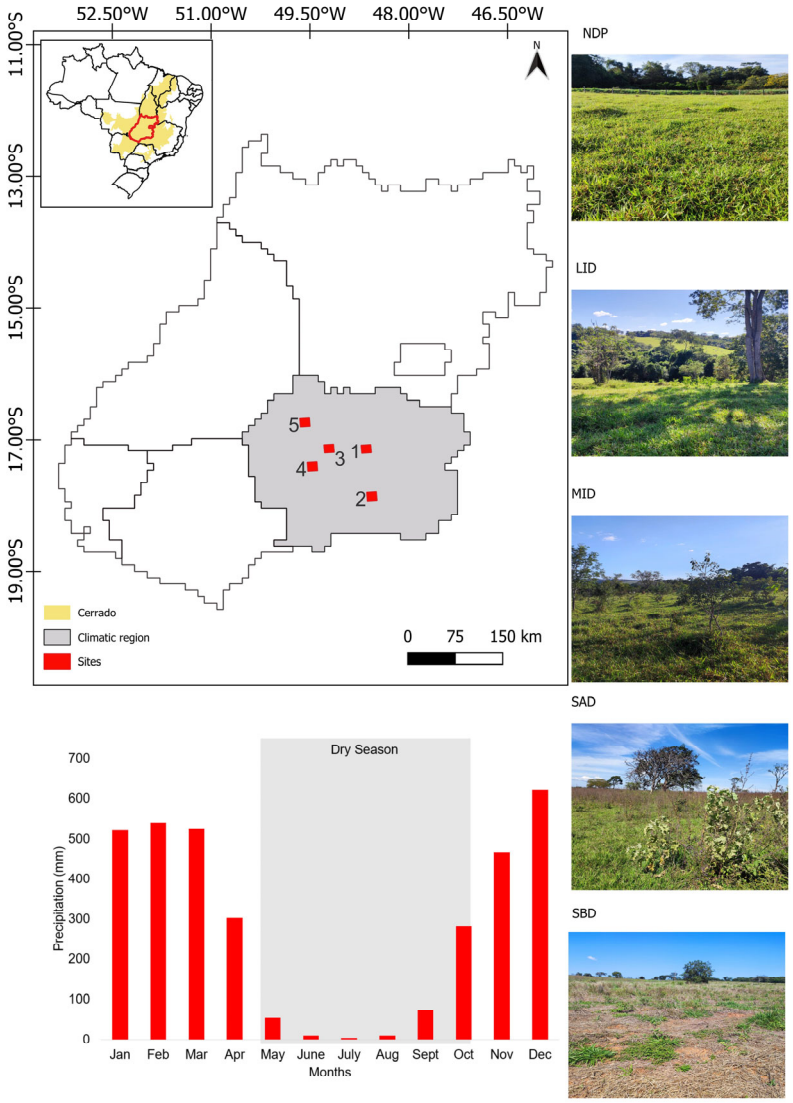


Figure 2. Location of the five sites (15 × 15 km each) selected in the southeastern region of the Brazilian state of Goiás in a climatically homogeneous region. The insets show photographs representative of non-degraded pasture (NDP) and of pastures with low-intensity degradation (LID), moderate-intensity degradation (MID), severe agronomic degradation (SAD), and severe biological degradation (SBD). The sites are numbered according to the municipality where they are located: 1. Bela Vista de Goiás; 2. Caldas Novas; 3. Piracanjuba; 4. Pontalina; and 5. Trindade. Long-term monthly precipitation (average values between 2001 and 2021) and the dry season period are also indicated for reference.

2.2. SuperDove Data Acquisition and Fieldwork Activities

Operating in a Sun-synchronous orbit at an altitude of 500 km, the PlanetScope SuperDove satellite constellation captures images across eight spectral bands spanning the 400–900 nm range (© 2024 Planet Labs PBC, San Francisco, CA, USA). The bandwidth varies from 16 nm (red-edge band 7) to 50 nm (blue band 2) (Table 1). The SuperDove bands 1 and 5 are also referred to as the "Coastal blue" and "Yellow" bands, respectively. The SuperDove has a spatial resolution of 3.7 m, a radiometric resolution of 12 bits, and a temporal resolution of one day (Table 1). The images are obtained in frame sizes of 32 km × 20 km [39].

Table 1. Spectral bands and resolutions of the PlanetScope SuperDove instrument.

SuperDove Band Number	Spectral Band	Spectral Positioning (nm)	Band Center (nm)	Bandwidth (nm)	Spatial Resolution (m)	Radiometric Resolution (bits)
1	Blue I (Coastal)	431–452	441	21	3.7	12
2	Blue II	465–515	490	50	3.7	12
3	Green I	513–549	531	36	3.7	12
4	Green II	547–583	565	36	3.7	12
5	Red I (Yellow)	600–620	610	20	3.7	12
6	Red II	650–680	665	30	3.7	12
7	Red-Edge	697–713	705	16	3.7	12
8	Near-infrared (NIR)	845–885	850	40	3.7	12

Source: Adapted from Galvão et al. [39] and from information provided by Planet Labs PBC (www.planet.com, accessed on 15 January 2024).

This study employed the surface reflectance product (level 3B) from the PlanetScope SuperDove satellite constellation for data analysis. The product includes images that undergo geometric, radiometric, and atmospheric corrections. The algorithm used for atmospheric correction is based on the 6S radiative transfer code. The algorithm uses lookup tables (LUTs) for standard atmospheric models and ancillary near real-time information from MODIS (e.g., water vapor, ozone, and aerosol data) to convert at-sensor radiance into surface reflectance SuperDove data (© 2024 Planet Labs PBC.). Surface reflectance images were downloaded from the Planet platform (https://www.planet.com, accessed on 15 May 2023). An available cloud mask, derived from band threshold values, provided information on areas potentially affected by clouds and their related shadows. However, to reduce uncertainties in the data analysis, we downloaded only images exhibiting a maximum of 20% cloud cover in the scene for subsequent scrutiny of their visual quality. Only cloud-free data were considered for the subsequent analyses.

Therefore, our analysis concentrated on 259 cloud-free images acquired across all sites from January to December 2022. This period was characterized by a notably increased availability of SuperDove images compared to the years 2020 and 2021. Figure 3 reveals significant gaps in cloud-free image availability during the initial 50 days of the year and from Day of the Year (DOY) 326 onwards. During these periods, there were extensive intervals of total image absence across all sites, attributed to the prevalence of cloud cover.

Field surveys were conducted in the designated sites during the years 2022 and 2023 to assess the presence of both degraded and non-degraded pastures. Employing an existing pasture mask and a meticulous statistical sampling design, which considered the spatial distribution of pastures within each site and their proximity to roads, all five sites were physically visited. A comprehensive total of 109 plots, representing distinct levels of degradation, were systematically sampled during the field surveys.

Following the methodology proposed by Teles [40], the field-sampled plots were categorized into five classes: non-degraded pasture (NOD) and pastures exhibiting low-intensity degradation (LID), moderate-intensity degradation (MID), severe agronomic degradation (SAD), and severe biological degradation (SBD). This classification method was designed with the purpose of distinguishing between the type and severity of pasture degradation. We adopted the original definition of degraded pastures by Dias-Filho [5], which comprises: (a) agronomic degradation, characterized by weed presence and secondary succession development of savannas; and (b) biological degradation, involving the decline in soil quality and aboveground biomass. Following the protocol outlined by Teles [40], we assessed all field plots using a scoring system ranging from one to seven, evaluating parameters such as development stage, weed incidence, termite mound presence, soil coverage, forage availability, current pasture condition, and productive potential. Expert pasture managers and forage production specialists determined specific score thresholds for each degradation class based on their extensive experience in discerning the

transition points between different degradation states. The field surveys covered 28 plots for NDP, 24 for LID, 38 for MID, 6 for SBD, and 13 for SAD.

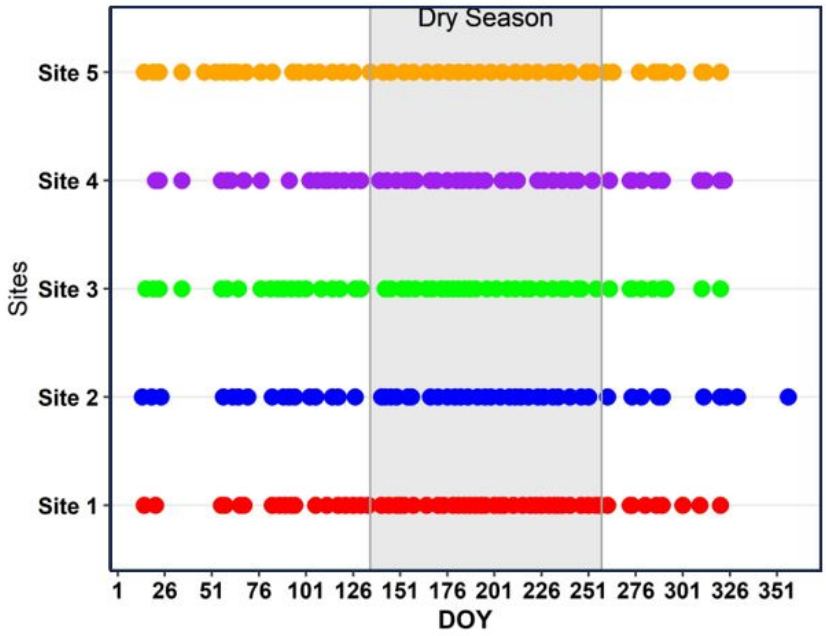


Figure 3. Frequency of cloud-free images captured by the SuperDove satellite constellation in 2022 for each of the five selected sites targeted for analysis. The dry season period is indicated for reference.

2.3. Selecting an Optimal Period for Discriminating Degraded Pastures

This study employed a pasture mask specific to the Cerrado biome, prepared by the Image Processing and Geoprocessing Laboratory of the Federal University of Goiás (LAPIG/UFG). The construction of this mask involved utilizing data acquired in 2020 by the MSI/Sentinel-2, supplemented by field information [1]. To align this mask with the spatial resolution of SuperDove and the specific year under consideration (2022), it underwent editing through visual interpretation using the Quantum GIS (QGIS) software (v3.36.3).

To identify the most suitable period for discriminating between the five classes of pasture degradation under investigation in this study (NDP, LID, MID, SAD, and SBD), we initiated the analysis by examining color composites of SuperDove images captured during both the rainy and dry seasons of 2022. Then, the average seasonal reflectance of each class, as measured by SuperDove, was plotted against the DOY in 2022. To compute the average reflectance, pixels were randomly sampled within the plots visited in the field. In cases of vegetation heterogeneity, degraded classes were oversampled as needed. The Mahalanobis distance, calculated using the eight reflectance bands of SuperDove, was employed to assess the dissimilarity between pairs of classes. All possible class pairs were taken into consideration, encompassing even the most similar ones, such as LID and MID.

2.4. Determination of SuperDove Attributes

After identifying the most suitable period for discriminating between the five classes of pasture degradation, we calculated some spectral and spatial attributes from SuperDove data (Table 2).

Given the SuperDove band configuration outlined in Table 1, various vegetation indices can be computed. Following the approach proposed by Galvão et al. [39], we calculated five vegetation indices for subsequent examination of their efficacy in discriminating pasture degradation classes: EVI, GRND, MPRI, NDVI, and REND. Their equations and references are shown in Table 3.

Table 2. Spectral and spatial attributes of the SuperDove data selected to assess their variations with different levels of pasture degradation.

SuperDove Attribute	Metric
Spectral	I. Surface reflectance of the eight SuperDove bands
	II. Five vegetation indices (EVI, GRND, MPRI, NDVI and REND)
	III. Four endmember fractions from SMA (NDP, SAD, SBD, and shade)
Spatial	Eight GLCM texture metrics calculated from the NIR band (texture mean, variance, homogeneity, contrast, dissimilarity, entropy, second moment and correlation)

Table 3. Suite of vegetation indices (VIs) selected for the data analysis. The original formulations were adjusted to the band positioning of the SuperDove instrument. Bands 2 (Blue band II centered at 490 nm), 3 (Green band I at 531 nm), 4 (Green band II at 565 nm), 6 (Red band I at 665 nm), 7 (Red-Edge band at 705 nm), and 8 (NIR band at 850 nm) were employed in the equations. The reflectance is denoted by 'p' in the equations, and the abbreviations for the VIs are defined in the text.

VIs	Equation	Reference
NDVI	$(pNIR_{b8} - pRed_{b6})/(pNIR_{b8} + pRed_{b6})$	Rouse et al. [37]
EVI	$2.5 \times (pNIR_{b8} - pRed_{b6})/(pNIR_{b8} + 6 \times pRed_{b6} - 7.5 \times pBlue_{b2}) + 1$	Huete et al. [34]
MPRI	$(pGreen_{b4} - pGreen_{b3})/(pGreen_{b4} + pGreen_{b3})$	Gamon et al. [42]
REND	$(pNIR_{b8} - pRe_{b7})/(pNIR_{b8} + pRe_{b7})$	Gitelson et al. [36]
GRND	$(pGreen_{b4} - pRed_{b6})/(pGreen_{b4} + pRed_{b6})$	Moura et al. [35]

The selection of these five vegetation indices is grounded in their biophysical significance. For example, as discussed by Galvão et al. [39] and Haddad et al. [29], EVI is particularly sensitive to vegetation structure. It addresses limitations of NDVI related to signal saturation over dense vegetation or the influence of soil background over sparse vegetation [29,34,37]. Conversely, GRND is potentially responsive to leaf flushing [35], capturing seasonal changes in new foliage. Following Galvão et al. [39], the equation adopted in Table 3 for calculating MPRI is a variant of the original formulation proposed by Gamon et al. [42], designed to transform negative values of this index into positive ones. MPRI is potentially sensitive to alterations in carotenoid pigments in live foliage, serving as a proxy for photosynthetic light use efficiency or vegetation productivity and stress [42]. Lastly, REND explores the red-edge interval, depicting the spectral transition from chlorophyll absorption to leaf-canopy scattering [36,38].

Endmember fractions were considered in the current study because most areas of biologically degraded pastures have soil exposure to the satellites. In this study, the SMA was preceded by employing the Sequential Maximum Angle Convex Cone (SMACC) technique to automatically identify spectral endmembers for constructing the model. The methodology described by Gruninger et al. [43] uses residual minimization (convex cone model) to find pixels with contrasting brightness in the scene, which are defined a priori as candidate endmembers. The algorithm is implemented in the Environment for Visualizing Images (ENVI) software (L3Harris Geospatial Solutions, Inc., Manila, Philippines, 2022, version 5.6.3). SMACC was applied to the surface reflectance of the eight SuperDove bands of the field-visited plots, with the maximum number of endmembers set to four for the sake of model simplicity. The unmixing Root Mean Squared Error Tolerance was set to 0.01, and endmember spectra were constrained to positive values at any wavelength. To merge candidate endmembers with reflectance spectra of similar shape, the Spectral Angle Mapper (SAM) technique was integrated into the SMACC algorithm. A threshold angle of 0.10 radians was selected for this purpose. Using the SMACC-derived endmember spectra, selected over plots of NDP, SAD and SBD, and a synthetic shade spectrum [44],

the SMA estimated the relative proportions of these four components on a per-pixel basis. The model assumes that the reflectance of a given pixel is a linear combination of these endmembers [45].

Finally, spatial attributes encompassed texture metric signals derived from the GLCM methodology [46]. In our analysis using the GLCM approach, the focus was on SuperDove's NIR band 8. We computed eight GLCM metrics, employing small window sizes of 3×3 pixels and an offset of one pixel, as recommended by previous studies [47,48]. These metrics include texture mean, variance, homogeneity, contrast, dissimilarity, entropy, second moment, and correlation. The definitions and interpretations of these texture metrics are detailed by Haralick et al. [46] and Zhou et al. [48].

2.5. Random Forest, Validation, and Test of Different Classification Scenarios

The concluding phase of the data analysis involved the RF classification of pasture plots within the SuperDove images. The classification was executed using the attributes individually, such as reflectance, vegetation indices, SMA endmember fractions, and GLCM texture metrics, as well as in combination. These attributes were computed from the SuperDove image representing the most suitable period for discriminating the pasture degradation classes.

Utilizing the Ranger package within the R software environment (v4.4.0), a unified model was constructed for all sites with an ntree parameter set to 1000 and an mtry parameter established as the square root of the total number of predictor variables. To circumvent spatial autocorrelation, a minimum distance criterion of three pixels was instituted for class sampling. The model incorporated a total of 3000 pixels, with 70% of the samples allocated for training and the remaining 30% for validation. Using the set of validation pixels, error matrices and the corresponding metrics, including overall classification accuracy (OA), Kappa, Precision (P), Recall (R), and F1-score (F1), were computed. The F1-score, a metric assessing the overall performance of a classification model by balancing Precision and Recall, takes into account false positives and false negatives, offering a comprehensive evaluation of the model's efficacy.

Using the complete set of attributes, this study explored two distinct classification scenarios: a more challenging one consisting of five classes (NDP, LID, MID, SAD, and SBD), and a less complex yet still demanding scenario comprising three classes (NDP, SAD, and SBD). Examining these two scenarios is crucial due to their potential implications for funding strategies and policies in delineating priority areas for renewal or recovery.

3. Results

3.1. Seasonal Reflectance Differences between Pasture Degradation Classes

Examination of false color composites from SuperDove imagery has revealed initial challenges in distinguishing between classes of pasture degradation during the dry season in the Cerrado region. Notably, an increase in NPV towards the dry season (DOY 227 in Figure 4) has posed difficulties in differentiating non-degraded pastures (NDP) from biologically degraded areas (SBD) characterized by high soil exposure. Consequently, the transition from the rainy to the dry season has led NDP plots to shift in color from orange (DOY 62) to cyan (DOY 227) in the false color composites (Figure 4). This shift is attributed to the spectral reflectance similarity between NPV and soil, and to the increasing amounts of NPV towards the dry season. Conversely, a reverse color pattern was observed with the onset of a new rainy cycle in October and November, marked by the prevalence of reddish shades in NDP plots (DOY 324 in Figure 4).

The observed pattern in the SuperDove color composites was corroborated through the analysis of the seasonal average reflectance in 2022 for the field-visited plots. Differences between pasture degradation classes were more pronounced during the rainy season than in the dry season, as illustrated in Figure 5a,b with the red and NIR bands 6 and 8, respectively. The transition from the rainy to the dry season (May to June) and the beginning of a new seasonal cycle between September and October emerged as particularly suitable periods

for effectively distinguishing between these classes. In the SuperDove red band, the class most effectively discriminated was SBD during the transition from the rainy to the dry season (and vice versa). This discrimination was attributed to the substantial soil exposure sensed by the satellite constellation during this period. In contrast to the increase in red reflectance (Figure 5a), a decrease in NIR reflectance was consistently observed over SBD plots throughout most of the seasonal cycle (Figure 5b).

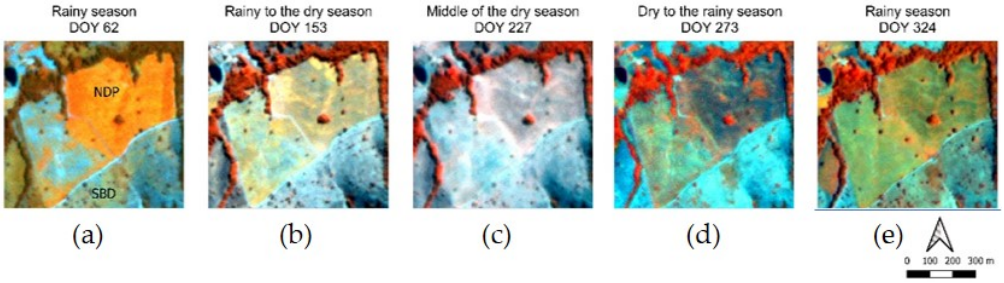


Figure 4. False color composites generated from SuperDove imagery, illustrating visual distinctions between plots of biologically degraded (SBD) and non-degraded (NDP) pastures across various seasonal stages. Notable time points include the rainy season (DOY 62 and 324 in (**a**,**e**)), the transition from the rainy to the dry season (DOY 153 in (**b**)), the middle of the dry season (DOY 227 in (**c**)), and the transition from the dry to the rainy season (DOY 273 in (**d**)). SuperDove bands 8 (NIR), 7 (red-edge) and 6 (red) are shown in red, green and blue colors, respectively.

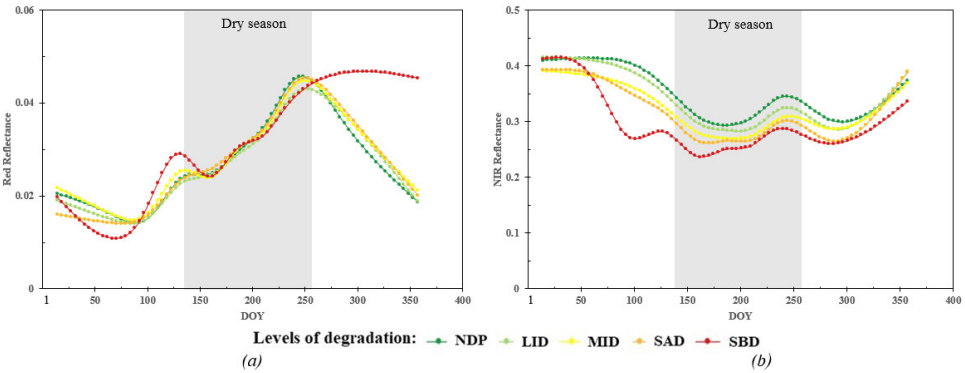


Figure 5. Seasonal variations in mean reflectance for both (**a**) red and (**b**) near-infrared (NIR) bands (SuperDove bands 6 and 8) across different pasture degradation classes. The symbols within the profiles denote data acquisition in 2022 through the satellite constellation. Class abbreviations are defined in the text.

When we considered the reflectance of the eight SuperDove bands collectively to calculate the Mahalanobis distance between pairs of classes, the most significant spectral distances for discriminating between SAD and LID, as well as between SAD and MID, were noted at the onset of June (DOY 153 in Figure 6). Consistent with the pattern depicted in Figures 4 and 5, the second most substantial distance between these classes occurred at the beginning of the rainy season (new seasonal cycle) in October (DOY 273). Conversely, the smallest spectral distances between pairs of classes were observed in the middle of the dry season in July (DOY 227 in Figure 6). During this period, the reflectance of the SuperDove bands was predominantly influenced by the presence of non-photosynthetic vegetation (NPV) over the pasture plots.

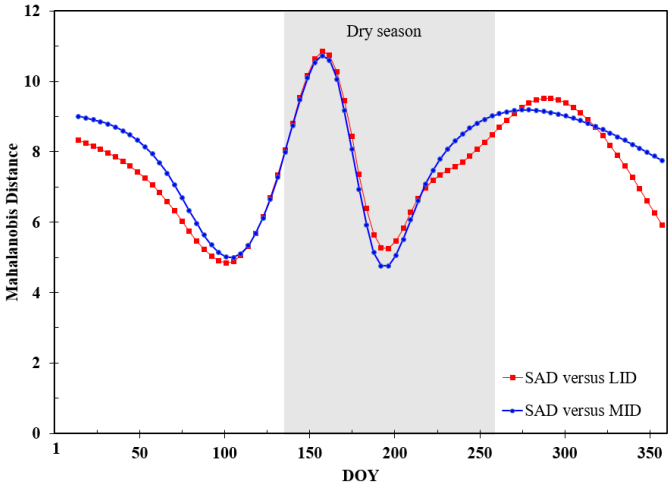


Figure 6. Seasonal variation in the Mahalanobis distance for discriminating areas of Severe Agronomic Degradation (SAD) from those with Low- (LID) and Moderate-intensity (MID) degradation using the eight-band reflectance data from SuperDove.

3.2. Discriminative Ability of the Spectral and Spatial Attributes

Given the significant reflectance differences observed between class pairs during the transition from the rainy to the dry season, as detailed in the preceding section on Mahalanobis distance results, our exploratory analysis investigated the discriminative ability of the spectral and spatial attributes. We focused the RF classification on data acquired by SuperDove over the five sites on 2 June 2022 (DOY 153). During this date, when the SMA was applied to pasture plots across all sites representing the five classes of pasture degradation, the technique automatically detected three endmembers. These endmembers consisted of two pixels of green vegetation (GV1 and GV2) and one pixel of bare soil (S). Along with a synthetic shade spectrum, these were considered to compose a four-endmember model. Upon locating these pixels in the images, we observed that the first endmember originated from an area of non-degraded pasture (green line in Figure 7), while the other two were retrieved from areas of severe agronomic (blue line) and severe biological (red line) degradation, respectively. When compared to areas of SAD and SBD, areas of NDP exhibited better-defined chlorophyll absorption bands around 660 nm and higher reflectance in the NIR interval due to leaf scattering (Figure 7). NDP displayed a more homogeneous vegetation cover, in contrast to SAD, characterized by a heterogeneous mixture of pasture leaves and invasive plant species, accounting for the observed differences in Figure 7. The endmember reflectance spectrum of SBD (red line in Figure 7) closely resembled that of bare soil, lacking any spectral features of green leaves.

Employing these endmember spectra along with the synthetic shade spectrum (Figure 7), SMA fraction images were created for the five sites. The fraction values of the endmembers served as input data for the RF classification. Consequently, the SMA model comprised GV1 (Green Vegetation 1), GV2 (Green Vegetation 2), soil (S), and shade, which were approximately equivalent to plots representing endmembers of NDP, SAD, SBD, and shade, respectively.

In addition to reflectance and SMA fractions, another spectral attribute indicating differences between degraded and non-degraded pastures was that of vegetation indices. For example, the relationship between NDVI and GRND showed an approximate linearity (Figure 8a). Classes with severe degradation, especially biological degradation (SBD), exhibited, on average, lower NDVI and GRND compared to non-degraded pastures (NDP). This result is anticipated, given that SBD typically displays high red and green reflectance along with a low NIR response in comparison to other classes (Figure 5). Conversely, the prevalence of green leaves in non-degraded pastures leads to an increase in reflectance in the green band and a decrease in the red band (chlorophyll absorption). When considering other VIs in the analysis, a similar pattern emerged between degraded and non-degraded pastures. For instance, SBD generally exhibited lower values of EVI and REND than NDP

due to the significant proportions of soil fractions sensed by SuperDove over biologically degraded plots (Figure 8b).

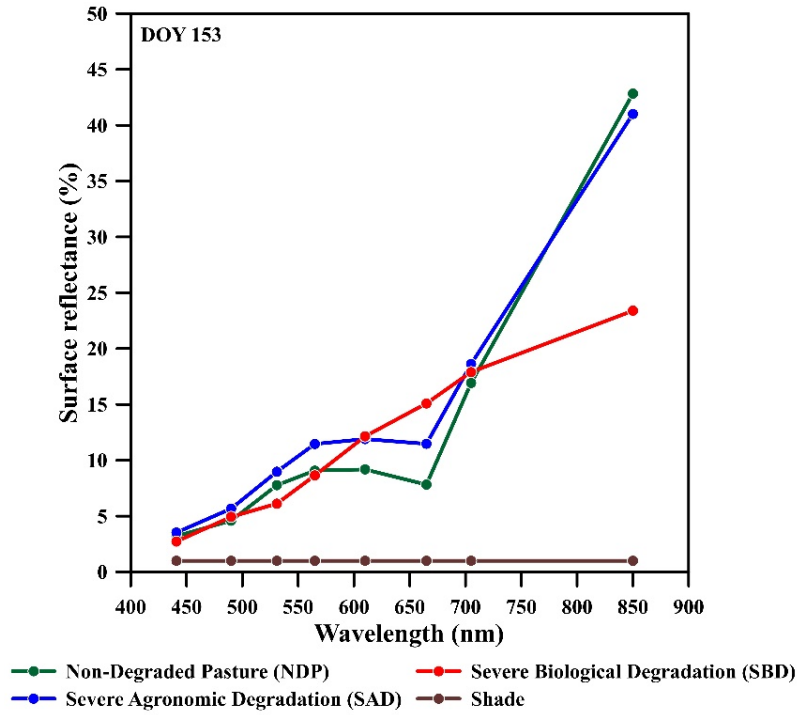


Figure 7. Endmember reflectance spectra derived from Sequential Maximum Angle Convex Cone (SMACC) for SuperDove data acquired on 2 June (DOY 153) over areas exhibiting varying degrees of pasture degradation across the five studied sites in central Brazil.

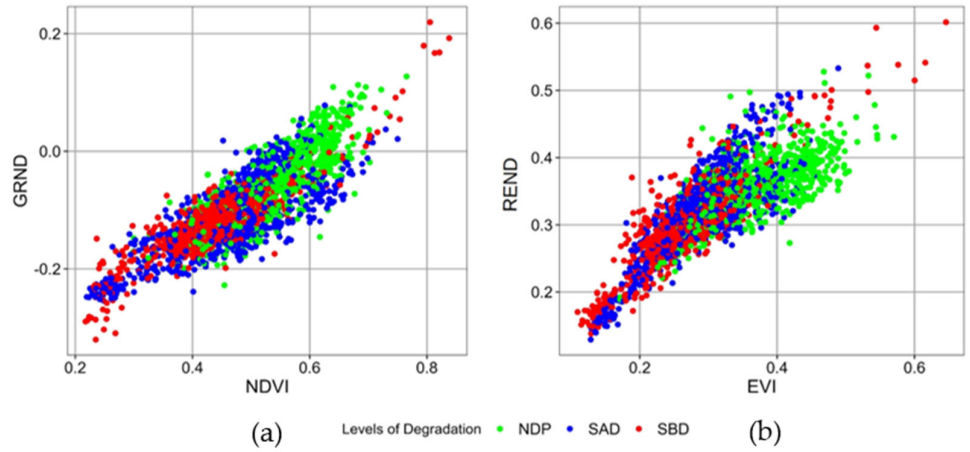


Figure 8. Scatterplots illustrating the relationships between (**a**) NDVI and GRND and (**b**) EVI and REND for three field-sampled classes of pasture degradation: Non-degraded pasture (NDP) and pastures with severe agronomic (SAD) and biological (SBD) degradation.

Both the SMA fractions and the vegetation indices exhibited close relationships with each other. For example, regions with spectral mixtures featuring high abundance values of GV1 (red color in the SMA middle panel of Figure 9) also demonstrated elevated NDVI values (sea green color in the NDVI right panel of Figure 9). Conversely, pasture plots characterized by a high abundance of soil (blue color in the SMA middle panel of Figure 9) displayed low NDVI values (orange color in the NDVI right panel of Figure 9). Consequently, GV1 showed a positive relationship with NDVI, while the soil fraction exhibited an inverse correlation with this index. In the SMA color composite, less degraded pastures

were distinctly delineated by shades of green vegetation, whereas severe degradation, particularly of a biological nature, was more prominently detected by the blue color in the soil fraction image.

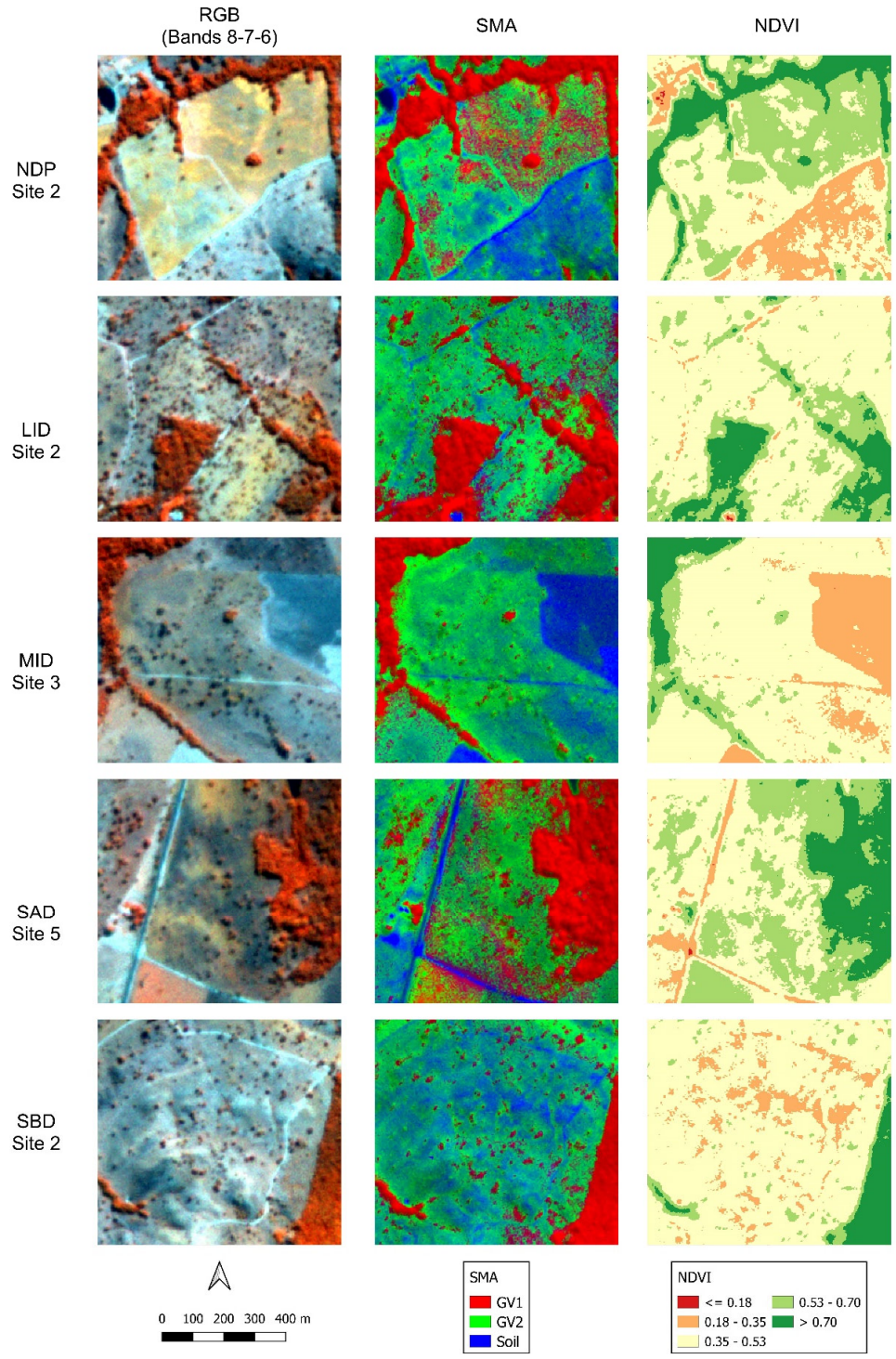


Figure 9. False color composites (SuperDove bands 8, 7, and 6 in RGB) illustrating examples of the five classes of pasture degradation (NDP, LID, MID, SAD, and SBD) are presented on the left side of the figure. In the middle panel, color composites of green vegetation (GV1), GV2, and soil (S) fraction images in RGB are displayed. Lastly, NDVI images are presented on the right side.

Finally, the analysis of GLCM texture metrics for the NIR band of SuperDove revealed that this type of attribute could contribute to differentiating pasture degradation. For instance, examination of the two most common GLCM metrics showed a decrease in texture mean (Figure 10a) and variance (Figure 10b) over plots of severely degraded pastures (SAD and SBD). However, standard deviation values for both metrics generally decreased with degradation (Figure 10). Thus, pasture plots with exposed soils exhibited a more homogeneous texture than that observed over less degraded pastures. No well-defined patterns with degradation were observed for contrast, dissimilarity, energy, entropy, and correlation.

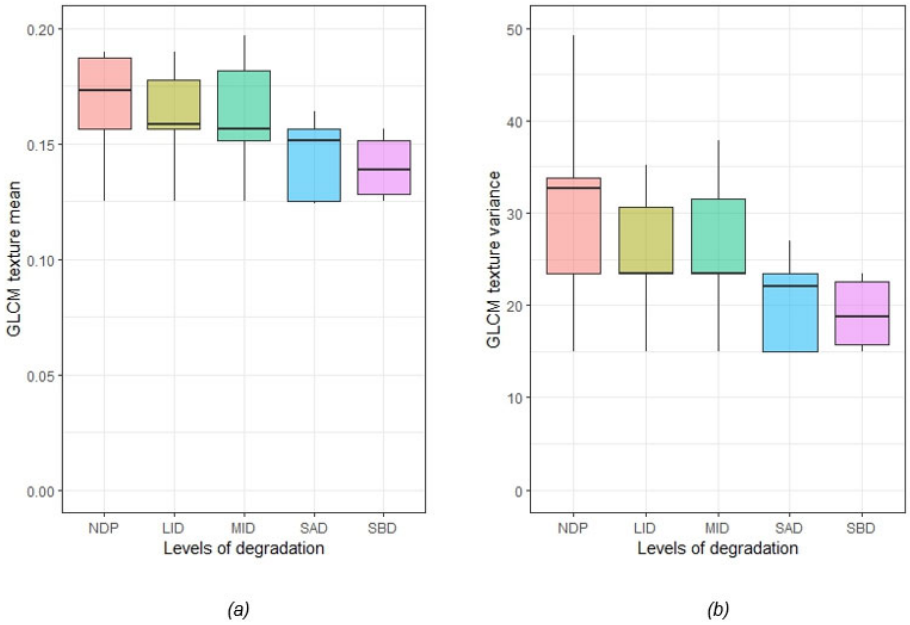


Figure 10. Variations in Gray Level Co-occurrence Matrix (GLCM) texture metrics, specifically (**a**) texture mean and (**b**) texture variance, calculated from the Near-Infrared (NIR) band 8 of SuperDove for the five classes of pasture degradation.

3.3. Random Forest (RF) Classification Using Individual Sets of Attributes

The RF classification performance was first assessed using individually eight-band reflectance values, four fraction images from SMA, five selected vegetation indices, and eight GLCM texture metrics to distinguish among the five classes of pasture degradation (NDP, LID, MID, SAD, and SBD). The attributes were calculated from the image obtained on DOY 153 (2 June 2022).

Among the attributes, band reflectance of SuperDove yielded the highest F1-scores, as depicted in Figure 11. This outcome suggests that reflectance values exhibit robust predictive power, enabling the classification model to effectively differentiate between distinct classes. Utilizing reflectance data in RF, an overall classification accuracy (OA) of 0.66 was achieved, surpassing the values recorded with SMA (0.53) and vegetation indices (0.50). The GLCM texture metrics yielded the lowest values of OA (0.34). Among the five classes tested for classification, the highest F1-scores were observed for NDP and SBD, representing non-degraded and severely degraded areas, respectively.

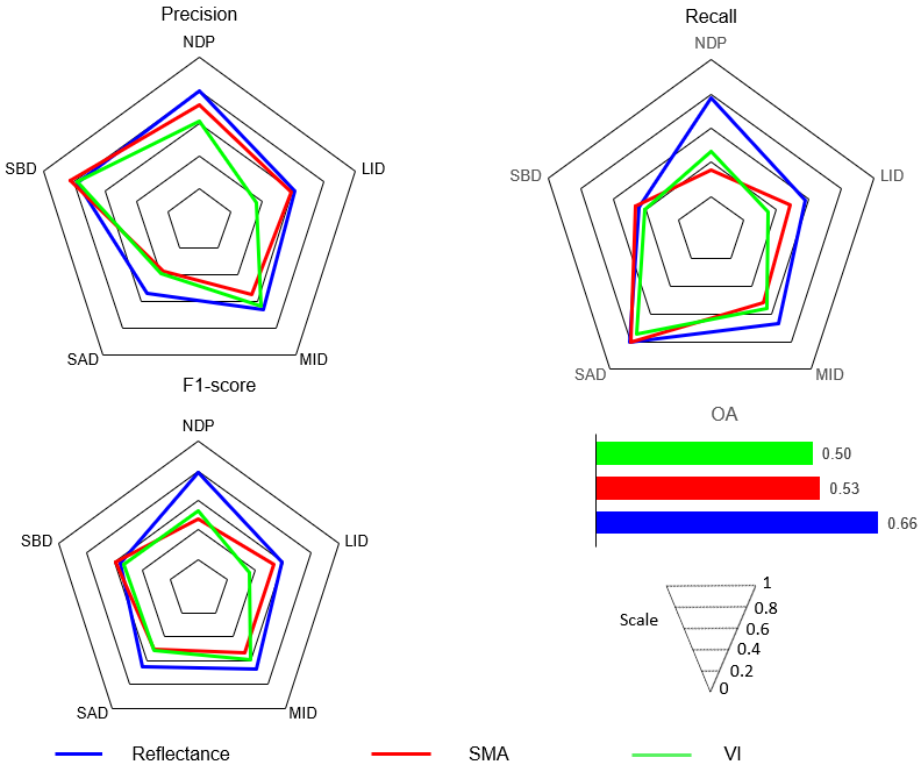


Figure 11. Variations in Precision, Recall, F1-score, and Overall Accuracy (OA) resulting from the Random Forest (RF) classification of five classes of pasture degradation (NDP, LID, MID, SAD, and SBD). The classifier utilized individual attributes, including the reflectance of the eight SuperDove bands, five vegetation indices (EVI, GRND, MPRI, NDVI, and REND), and four-endmember fractions from Spectral Mixture Analysis (SMA) (GV1, GV2, soil, and shade). Results from GLCM texture metrics were excluded for enhanced graphical representation. The reported results refer to the validation dataset.

3.4. Random Forest (RF) Using Combined Sets of Attributes in Two Classification Scenarios

Despite its challenging and complex nature, the ability to discriminate among the five classes of pasture degradation (first classification scenario) is appealing. Areas characterized by low-to-moderate intensity degradation (LID and MID) can be strategically chosen, in terms of funding allocation, as priority areas for renewal or recovery efforts compared to severely degraded regions. However, the RF classification results presented in Table 4 using combined sets of attributes revealed that the highest F1-scores were achieved for the two severely degraded classes (0.71 for SAD and 0.88 for SBD).

Consequently, notable levels of confusion were evident between non-degraded pastures (NDP) and pastures at initial or moderate stages of degradation (LID and MID). These areas exhibited high variability in vegetation characteristics on their surfaces, such as plant height and composition, making their discrimination more challenging. While SBD stood out as the most distinctive class due to soil exposure, some degree of confusion with SAD was also noted, as indicated by Table 4.

When compared with the classification using only the reflectance attribute (Figure 11), the results from Table 4, utilizing the combination of metrics, showed an improvement in overall classification accuracy from 0.66 to 0.69. In terms of accuracy, notable differences were observed in the SAD and SBD classes, suggesting that utilizing all attributes reduces the likelihood of commission errors in these classes. Conversely, Recall was significantly higher in the classification using the combined attributes than in the one using individual attributes, particularly in the SBD class, achieving 0.9. This outcome indicates less confusion in the classification of this class with fewer false negatives.

Table 4. Confusion matrix resulting from the classification using the combination of spectral and spatial attributes in discriminating the five degradation classes.

	Reference				
	NDP	**LID**	**MID**	**SAD**	**SBD**
NDP	91	41	25	13	0
LID	29	96	47	9	0
MID	4	13	129	34	0
SAD	0	0	18	137	25
SBD	0	0	5	14	167
F1-score	0.61	0.58	0.64	0.71	0.88
Recall	0.53	0.53	0.72	0.76	0.90
Precision	0.73	0.64	0.58	0.66	0.87
Overall Accuracy (OA)	0.69				
Kappa	0.61				

Among the entire set of attributes, the top three most crucial variables for discriminating the classes were EVI, NDVI, and GRND. Soil fraction from SMA and the reflectance of the red and NIR bands of SuperDove followed closely in terms of importance (Figure 12). In comparison, GLCM texture data associated with the NIR band held lower importance. Overall, concerning importance, vegetation indices accounted for 43.93% of the classification performance, while the reflectance of the SuperDove bands and the SMA fraction images contributed 28.51% and 21.33%, respectively. Texture metrics contributed only 6.23% to the discriminatory power, with a notable concentration in texture mean and variance (Figure 12).

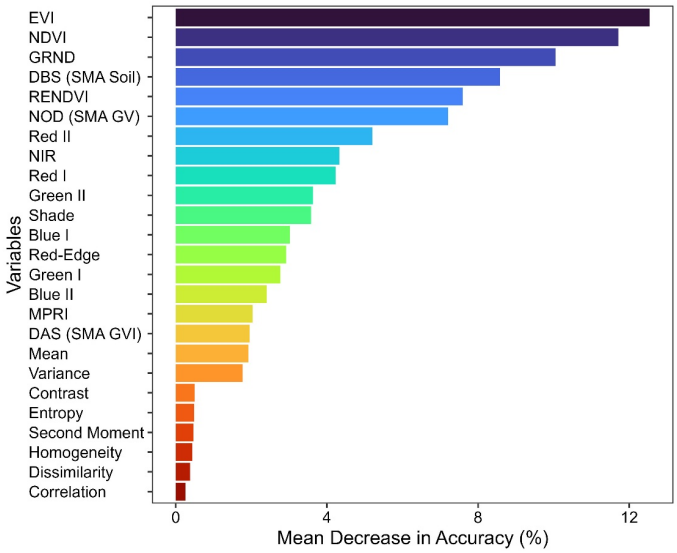


Figure 12. Percentage of importance assigned to each variable in the Random Forest (RF) classification of five classes of pasture degradation (NDP, LID, MID, SAD, and SBD).

Figure 13 presents various examples of RF classification for different study sites. A comparison with the ground truth map (Figure 13a) indicates that the RF classification, utilizing all five classes, demonstrated superior performance in non-degraded and severely degraded classes, represented by the green, orange, and red colors (NDP, SAD, and SBD in Figure 13b). However, notable confusions were evident in the low and moderate degradation classes, represented by light green and yellow colors (LID and MID, respectively). The former was frequently misclassified as NDP, and the latter showed confusion with NDP and SAD. In Figure 13c, the uncertainty map reveals higher uncertainties in areas identified as SBD that are in close proximity to non-degraded pasture. Additionally, uncertainties are

observed in regions where LID and MID occur since these classes exhibit greater similarities with other classes.

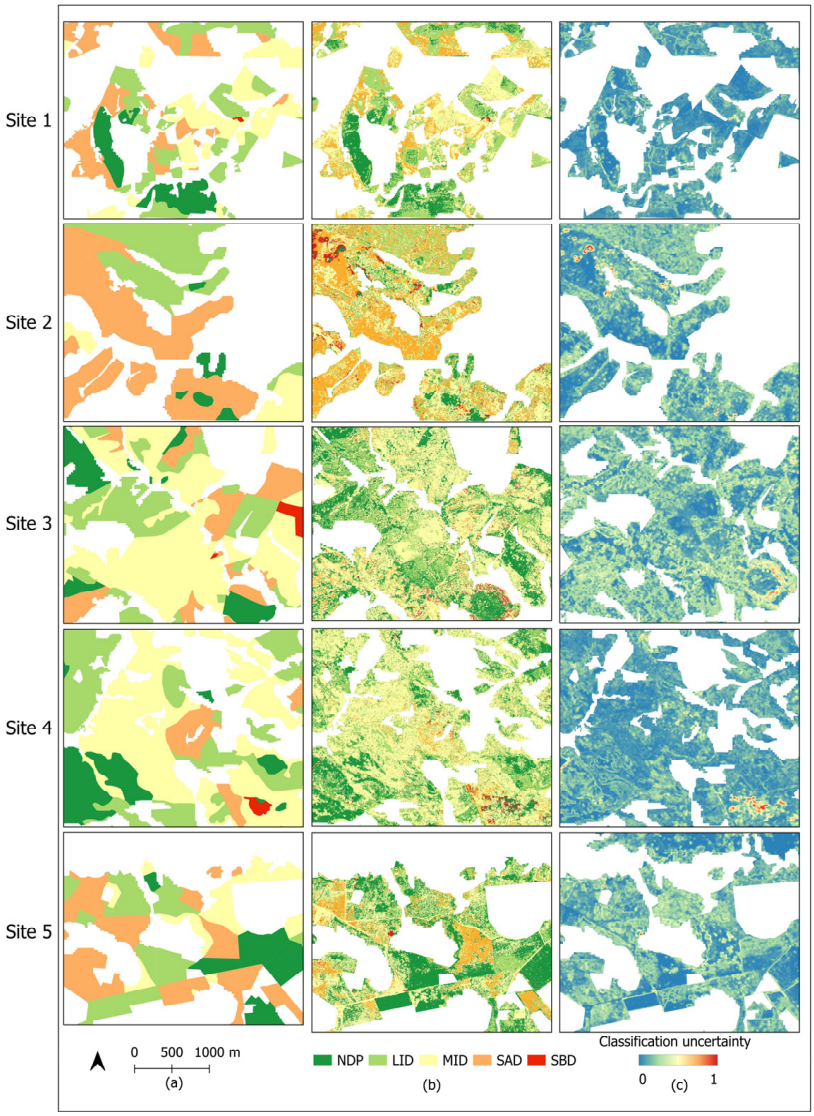


Figure 13. (**a**) Ground truth map and (**b**) Random Forest classification of degraded and non-degraded pastures. Classification uncertainties are depicted in (**c**). The abbreviations are defined in the text.

In the second classification scenario, all previously described input variables were utilized, but the classification considered only three classes: NDP and severe agronomic (SAD) and biological (SBD) pasture degradation. This approach was necessary to investigate whether the inclusion of intermediate classes (LID and MID) has a significant impact on the classification, as indicated before. Upon examining the confusion matrix (Table 5), it is evident that classes SBD and SAD exhibited confusions, albeit less pronounced than those seen in the classification using five classes. Additionally, there was confusion between the classes NDP and SAD. However, the accuracy metrics of the classifier with three classes (OA = 0.88) outperformed the previous classification with five classes (OA = 0.69), as expected. In the first classification scenario, LID and MID were sources of significant confusion, with the former being frequently confused with the NDP class and the latter with the SAD class.

Table 5. Confusion matrix resulting from the classification using the combination of spectral and spatial attributes in discriminating three degradation classes: non-degraded pasture (NDP) and pastures with severe agronomic (SAD) and biological (SBD) degradations.

	Reference		
	NDP	**SAD**	**SBD**
NDP	160	20	0
SAD	11	138	31
SBD	0	2	178
F1-score	0.91	0.81	0.91
Recall	0.89	0.77	0.99
Precision	0.93	0.89	0.91
Overall Accuracy (AO)	0.88		
Kappa	0.81		

4. Discussion

This inaugural study utilizing high spatial and temporal resolution data from the eight-band PlanetScope SuperDove satellite constellation considered two distinct classification scenarios of pasture degradation within the Brazilian savanna ecosystem. The first scenario, a more intricate one, encompasses five classes of pasture degradation (NDP, LID, MID, SAD, and SBD). Meanwhile, the second scenario involves a more streamlined classification, considering only three classes of degradation (NDP, SAD, and SBD). By incorporating a pre-existing pastureland mask and delving into the discrimination of five pasture degradation classes (scenario 1), we have elevated the analysis to a higher level of complexity. The inclusion of low- to moderate-intensity classes of degradation (LID and MID) in the analysis is particularly noteworthy due to the comparatively lower costs associated with the recovery or renewal of these areas compared to severely degraded areas. Notably, the Brazilian government, with the aim of rehabilitating 15 million hectares of degraded pastures by 2030, is supporting such efforts through subsidized credits to facilitate management and fertilization actions [13].

Due to the reduction in the number of classes in the second classification scenario and the apparent simplification of the analysis, the overall accuracy increased from 0.69 (scenario 1) to 0.88 (scenario 2) when employing the combined sets of spectral and spatial attributes. When compared to non-degraded or severely degraded pastures, classes with low-to-moderate-intensity degradation (LID and MID) exhibited greater variability in the field, contributing to misclassifications. In these instances, both agronomic and biological degradation processes were detected in pasture plots with MID, leading to variable proportions of green vegetation (invasive plants) and exposed soils for the satellite constellation. Consequently, this variability introduced spectral changes in the attributes measured by the SuperDove, making MID the class with the lowest Precision (0.58) in the RF classification.

Another contribution of this study, stemming from the PlanetScope SuperDove satellite constellation's ability to generate densely spaced time series, lies in the identification of optimal periods for remote sensing discrimination of pasture degradation. In comparison to the dry season, more favorable scenarios for discriminating pasture degradation were observed during the rainy season or in transitional periods between both seasons. For example, in the middle of the dry season, classification accuracy metrics were comparatively lower (OA = 0.20 for DOY 227 in Figure 14) than the values observed in the transition from the rainy to the dry season (OA = 0.69 for DOY 153 in Figure 14).

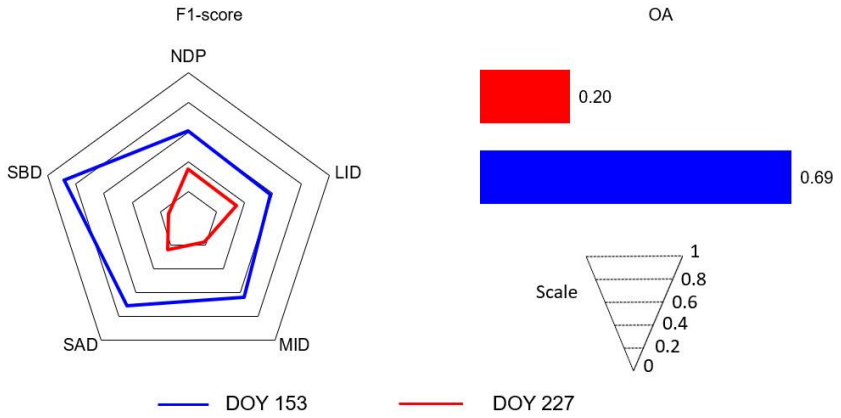


Figure 14. Variations in F1-score and Overall Accuracy (OA) resulting from the Random Forest (RF) classification of five classes of pasture degradation (NDP, LID, MID, SAD, and SBD) using the combined sets of attributes. Results are presented for two dates representing the transition from the rainy to the dry season (DOY 153 in June; blue color results) and the middle of the dry season (DOY 227 in August; red color results). The reported results refer to the validation dataset.

Our study, therefore, has identified suitable periods for data acquisition, notably the transition from the rainy to the dry season (May to June) and the beginning of a new seasonal cycle in October after the initial rainfall events. Compared to the peak of the rainy season (January–February), these transitional periods offer better opportunities for acquiring cloud-free data over the studied sites. In agronomic degradation, shifts in botanical composition lead to decreased forage productivity and increased weed infestation [5]. Depending on the frequency of cattle presence and grazing conditions, weeds may vary in incidence and height. Because of the different sensitivities to precipitation or water stress, the reflectance of pasture species and weeds can differ seasonally to the satellites in the transitional periods between rainy and dry seasons, facilitating their discrimination. Conversely, in biological degradation, a significant decline in aboveground forage biomass is typically observed, often revealing patches of degraded exposed soils sensed by satellites across pasturelands. Due to the marked decrease in vegetation productivity, pastures exhibiting signs of severe biological degradation displayed greater sensitivity to water stress compared to non-degraded pastures, manifesting earlier reflectance changes in the visible and near-infrared bands (VNIR) than other classes. Similarly, earlier reflectance modifications in SuperDove spectra were noted at the onset of the rainy season over severely degraded areas. In ecosystems like the Cerrado, characterized by a prolonged dry season and a naturally less vigorous vegetation, due to soil and climate conditions, biological degradation is the predominant form [5]. Various pasture management strategies and techniques exist to recover or renew degraded pastures in the Brazilian savanna, with costs increasing in direct proportion to degradation levels [5,9–11]. In our study, this observation validates the approach of incorporating varying levels of degradation into our data analysis strategy.

During the dry season, distinguishing biologically degraded from non-degraded pastures is complicated by the presence of NPV or dry leaves covering the surfaces [49]. In non-degraded pastures, the relative proportions of NPV to GV observed by the SuperDove increase from the rainy to the dry season. Given the spectral similarity between NPV and soils in the VNIR interval [44], discriminating between NDP and SBD becomes more challenging in the dry season than in other periods of the seasonal cycle due to the increased amounts of NPV observed over non-degraded areas. In this context, incorporating Shortwave Infrared (SWIR) spectral bands into the analysis, particularly narrow bands within the 2100–2400 nm range from hyperspectral instruments, could enhance class separability between soil and NPV during the dry season.

In terms of spectral resolution, the SuperDove (PSB.SD) demonstrated significant improvements in band configuration compared to the other two generations of Cube-

Sats, which used to acquire images in four multispectral bands (PS2 and PS2.SD). Within the set of eight SuperDove bands, those situated in the red, red-edge, and NIR spectral intervals were identified by the RF algorithm as the most important for discriminating pasture degradation. Pastures with severe biological degradation exhibited distinct rates of change in the reflectance of these bands with increasing soil water stress, particularly when contrasted with other classes. As commonly observed in savanna grassland areas, a reduction in chlorophyll content and an increase in NPV generally lead to an increase in red reflectance and a decrease in NIR reflectance as the dry season progresses [28,50]. During the transition from the rainy to the dry season, non-degraded pastures display more green leaves and a well-defined 660-nm chlorophyll absorption band in SuperDove spectra, when compared to other pasture degradation classes (Figure 7). In comparison to biologically degraded areas having more exposed soils, the SuperDove spectra of non-degraded pastures also exhibited higher reflectance in the NIR range. This change can be attributed to the increase in leaf scattering (plant structure), resulting from gains in leaf area index (LAI) and aboveground biomass observed in NPD areas. In agronomical degradation, plant structure can vary based on the quantity, type, and height of palatable weeds for cattle, influencing NIR reflectance through changes in surface roughness detected by the satellite. The spectral effects of NPV, soils, and leaf tissue water content primarily manifest in the SWIR, which is not covered by the SuperDove bands. An illustration of this phenomenon is presented using Operational Land Imager (OLI)/Landsat-8 reflectance spectra for a period corresponding to the transition from the rainy to dry season in May (Figure 15a). In the OLI SWIR bands located close to 1650 nm and 2200 nm, the reflectance of SBD areas exceeds that observed in NDP and SAD areas. This difference is attributed to the reduced water content in leaf tissues and the increased presence of NPV and exposed soils in biologically degraded pastures viewed by the Landsat instrument.

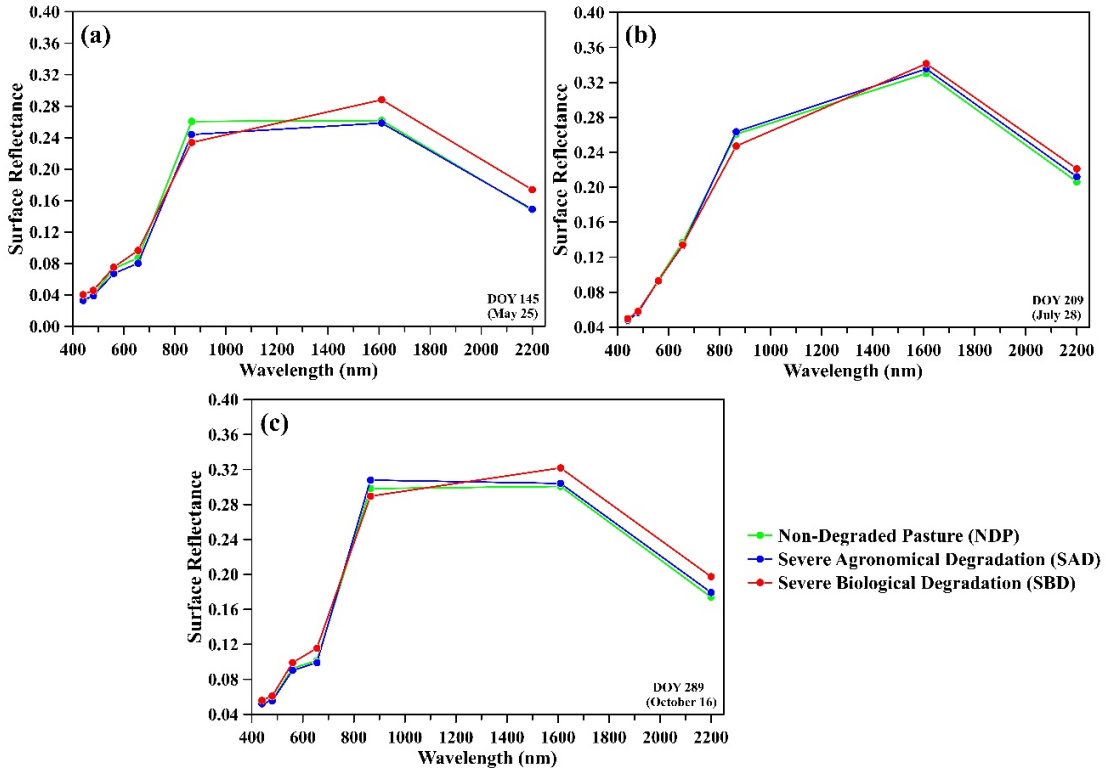


Figure 15. Average reflectance spectra from OLI/Landsat-8 data acquired over field-surveyed plots representing non-degraded pastures and pastures experiencing severe agronomical or biological degradation. The results are presented for various dates during the year 2021, specifically during (**a**) the transition from the rainy to the dry season, (**b**) the middle of the dry season, and (**c**) after the occurrence of the first rainfall events in the new seasonal cycle in October.

Upon preliminary examination of OLI/Landsat-8 spectra, the potential discriminatory power of the SWIR spectral region (around 1650 nm and 2200 nm) is evident (Figure 15). In a study focused on mapping pasture degradation in the Atlantic Forest biome, de Torres et al. [51] observed gains in classification accuracy upon incorporating SWIR bands into the data analysis. Inspection of Figure 15 also confirmed challenges in separability between degraded and non-degraded pastures, previously observed with the SuperDove instrument during the dry season. For instance, compared to the middle of the dry season (DOY 209 in Figure 15b), the discrimination of non-degraded pastures (NDP) from pastures with severe biological or agronomic degradations (SAD and SBD) is more feasible during the transition from the rainy to the dry season (DOY 145 in Figure 15a) or toward the new cycle of the rainy season in October (DOY 289 in Figure 15c).

Comparison of preliminary RF classification results for the five classes of degraded pastures (NDP, LID, MID, SAD, and SBD) utilizing reflectance data of 10 bands (10-m and 20-m spatial resolution) from the MSI/Sentinel-2 (400–2500 nm) and eight bands from the SuperDove (400–900 nm), both acquired between 2 and 4 June 2022, demonstrated enhanced overall classification accuracy with Sentinel-2 data (0.79 versus 0.66 in Figure 16). Consistent with the spectral patterns depicted in Figure 15 using Landsat data, these enhancements are likely to arise from the integration of SWIR data into the classification methodology, leading to the higher F1-scores observed for most classes in Sentinel-2 data compared to SuperDove observations (Figure 16). Hence, additional research is necessary to precisely determine the impact of SWIR bands on the classification efficacy of pasture degradation.

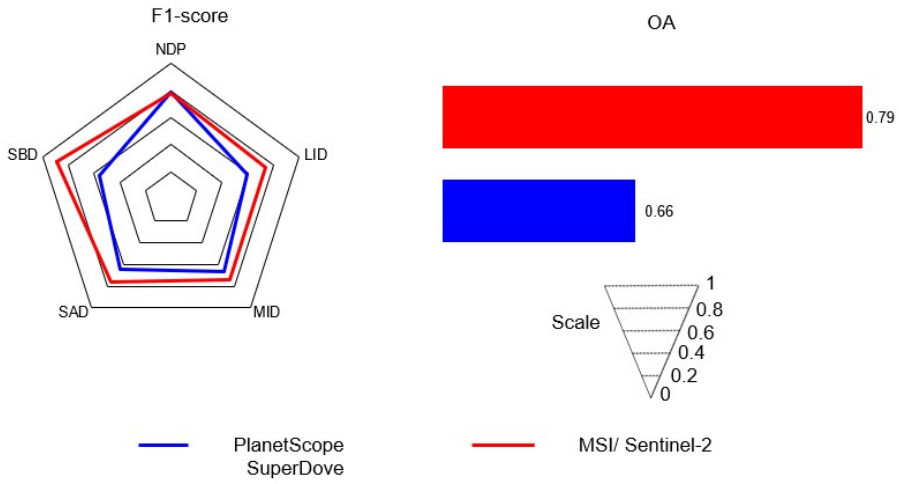


Figure 16. Variations in F1-score and Overall Accuracy (OA) resulting from the Random Forest (RF) classification of five classes of pasture degradation (NDP, LID, MID, SAD, and SBD) using reflectance data of 10 bands (10-m and 20-m spatial resolution) from the Multispectral Instrument (MSI)/Sentinel-2 (400–2500 nm) and eight bands from the SuperDove (400–900 nm). Images from both instruments were acquired in approximately coincident dates (2 and 4 June 2022). The reported results in blue (SuperDove) and red (MSI/Sentinel-2) colors refer to the validation dataset.

The acquisition of data in eight bands by the SuperDove enabled the determination of five vegetation indices (EVI, GRND, MPRI, NDVI, and REND), each having different biophysical sensitivities. In the RF classification, the three most important vegetation indices were identified as EVI, NDVI, and GRND, with each accounting for at least 10% of importance. In alignment with our findings, EVI was deemed the most effective vegetation index for distinguishing non-degraded pastures from those with invasive plants or palatable species (indicative of agronomic degradation) by Karnieli et al. [52]. Due to its strong dependence on NIR reflectance responses, EVI exhibits increased sensitivity to changes in vegetation structure and in the amounts of dry leaves or NPV over the pasture surfaces [39]. The second most influential vegetation index in our study was NDVI, which was also employed in trend analysis by Pereira et al. [11] for mapping degraded pastures

in the Cerrado biome using MODIS data. Lastly, GRND is likely to have captured changes in foliage within degraded and non-degraded areas in response to increasing water stress observed towards the dry season during the RF classification.

Endmember fractions derived from sub-pixel analysis of SuperDove data significantly improved the separability of severely degraded areas when compared to those with low-to-moderate intensity degradation. In the RF classification, compared to other fractions, the soil fraction exhibited the highest Mean Decrease in Accuracy value. This outcome was somewhat anticipated, given that soil cover was identified as one of the most crucial criteria for assessing degradation in the field [40]. High soil fractions were observed over degraded pastures, particularly in areas affected by biological processes of degradation.

In contrast to endmember fractions, most GLCM image texture metrics displayed limited importance in the classification. When compared to other classes, pastures with severe agronomic and biological degradation (SAD and SBD) exhibited lower values for NIR-band texture mean and variance, suggesting more homogeneous surfaces in these biologically and agronomically degraded areas. However, it is noteworthy that image texture metrics, when considered individually, demonstrated the poorest classification performance with an overall accuracy of 0.34, compared to the value of 0.66 obtained using only band reflectance. In this analysis, the entire set of SuperDove bands was not used to calculate the texture metrics; instead, the focus was on the NIR band. In this spectral interval, the energy incident over the pastures has higher transmittance through leaves and greater variability than that generated in the visible bands. In a study by Sano et al. [53], GLCM texture metrics derived from the entire set of PlanetScope bands have been successfully used for detecting double cropping areas in the Cerrado.

Our study has certain limitations that deserve consideration in future investigations. Notably, despite the PlanetScope SuperDove constellation's capability to acquire daily observations, the quality of the time series varied across the five studied sites due to cloud cover, resulting in gaps in the frequency of image acquisition, particularly in the first (January and February) and last (November and December) two months of the year. As a practical consequence of the cloud cover-related problem, we encountered challenges in interpolating the time series over each studied site, filling the gaps, and retrieving phenological metrics that could potentially contribute to the classification of degraded pastures. Given the varying sensitivity of savanna physiognomies to rainfall seasonality, information on vegetation phenology, derived from different vegetation indices calculated from the satellite constellation, can be important for savanna classification [28–30]. It is plausible that the incorporation of phenological metrics may enhance the classification accuracy of pastures, particularly in distinguishing severely degraded areas from other classes. However, in our present work, the time series was utilized solely to identify the most favorable periods for discriminating pasture degradation classes.

As another limitation of our work, we did not consider pasture species when defining the training and validation datasets, although the species were identified in the field. This decision was influenced by the predominant presence of *Brachiaria brizantha* in almost all surveyed pastures, making pasture species a less significant factor in introducing uncertainties into the classification results. Conversely, pasture management could potentially introduce spectral variability, especially in studies exploring interannual variations in vegetation indices associated with vegetation productivity or land degradation.

In our future investigations of pasture degradation, it is imperative to explore and test alternative machine or deep-learning approaches. However, in the savanna environment, numerous studies have consistently demonstrated the efficacy of RF in discriminating savanna physiognomies, outperforming other classifiers such as Support Vector Machine and Spectral Angle Mapper, or producing comparable results with deep learning approaches [27,29–31]. For instance, in a study aimed at differentiating pasture from non-pasture areas in Brazil, Parente et al. [31] reported F1-scores of 95% for RF, whereas a deep learning approach based on U-Net achieved 97% using the validation dataset. Given the substantial spectral similarity among the five classes of pasture degradation tested for

classification, it is essential to acknowledge that traditional approaches, such as Linear Discriminant Analysis (LDA), should not be overlooked in this context. Each method brings its own set of strengths and weaknesses. Exploring diverse techniques, metrics, and approaches ensures a comprehensive understanding of their applicability in addressing the specific challenges posed by pasture degradation classification in the savanna environment.

5. Conclusions

In alignment with our specific objectives, the following conclusions were drawn from the study:

(i) Enhanced discrimination between the five classes of pasture degradation in the Cerrado was observed during the rainy season compared to the dry season, particularly in the transition from the rainy to the dry season and the onset of a new seasonal rainy cycle in October. Challenges arise in the dry season due to the increased presence of non-photosynthetic vegetation in leaves and surfaces, posing difficulties in distinguishing non-degraded pastures from areas with biological degradation characterized by high soil exposure.

(ii) The classification using all attributes yielded an Overall Accuracy (OA) of 0.69, outperforming the use of individual datasets of reflectance (OA = 0.66), SMA (OA = 0.52), vegetation indices (OA = 0.38), and GLCM texture metrics (OA = 0.34). While the classification performance using VIs alone was not the most remarkable, the combined set of variables, including EVI, NDVI, and GRND, exhibited the highest importance in terms of Mean Decrease in Accuracy. Despite achieving accuracy with the combined set of variables and five classes (OA = 0.69), there were notable omissions and commissions, particularly in the intermediate classes of degradation (LID and MID).

(iii) The second classification scenario, focusing on severe degradation classes (SAD and SBD) and non-degraded pasture (NDP), demonstrated an increase in OA from 0.69 (five classes) to 0.88 (three classes). This result underscores the challenges associated with discriminating intermediate stages of degradation, a difficulty that is sometimes encountered even in the field.

Preliminary analysis of MSI/Sentinel-2 data and OLI/Landsat-8 reflectance spectra indicates the potential discriminatory power of SWIR bands to separate the classes of pasture degradation. An initial evaluation of RF classification outcomes for the five classes of pasture degradation using only reflectance data from MSI/Sentinel-2 (400–2500 nm) and SuperDove (400–900 nm), to ensure fair comparison of results, showed a significantly improved overall accuracy (0.79 versus 0.66) with Sentinel-2 data. This gain in OA is probably due to the insertion of SWIR Sentinel-2 spectral bands in the analysis. Further studies are necessary to confirm this evidence, as the SWIR bands are not covered by the PlanetScope SuperDove satellite constellation. Additionally, further investigations are needed to evaluate the potential discriminatory power of land surface phenology metrics to differentiate these classes.

Author Contributions: Conceptualization and data analyses, A.G.P.S., L.S.G. and L.G.F.J.; writing—review and editing, all authors. All authors have read and agreed to the published version of the manuscript.

Funding: This study was partially funded by the Coordenação de Aperfeiçoamento de Pessoal de Nível Superior—Brasil (CAPES)—Finance Code 001, and by the Conselho Nacional de Desenvolvimento Científico e Tecnológico (CNPq) (grant number 307792/2021-8).

Data Availability Statement: The shapefiles for the different sites are publicly available at the Laboratório de Processamento de Imagens e Geoprocessamento (LAPIG) from the Universidade Federal de Goiás (UFG) at the Pasture Atlas website (https://atlasdaspastagens.ufg.br/map, accessed on 15 May 2023). This resource includes not only the field points used in this study, but also additional data and maps.

Acknowledgments: We thank ©2022 Planet Labs Inc. for providing the images made available by the NICFI (Norway's International Climate and Forest Initiative). Comments by the anonymous reviewers and Editor are highly appreciated.

Conflicts of Interest: The authors declare no conflicts of interest.

References

1. Parente, L.; Mesquita, V.; Miziara, F.; Baumann, L.; Ferreira, L. Assessing the pasturelands and livestock dynamics in Brazil, from 1985 to 2017: A novel approach based on high spatial resolution imagery and Google Earth Engine cloud computing. *Remote Sens. Environ.* **2019**, *232*, 111301. [CrossRef]
2. Santos, C.O.d.; Pinto, A.d.S.; Silva, J.R.d.; Parente, L.L.; Mesquita, V.V.; Santos, M.P.d.; Ferreira, L.G. Monitoring of Carbon Stocks in Pastures in the Savannas of Brazil through Ecosystem Modeling on a Regional Scale. *Land* **2023**, *12*, 60. [CrossRef]
3. Santos, C.O.d.; Mesquita, V.V.; Parente, L.L.; Pinto, A.d.S.; Ferreira, L.G., Jr. Assessing the Wall-to-Wall Spatial and Qualitative Dynamics of the Brazilian Pasturelands 2010–2018, Based on the Analysis of the Landsat Data Archive. *Remote Sens.* **2022**, *14*, 1024. [CrossRef]
4. Kichel, A.N.; Miranda, C.H.B.; Zimmer, A.H. Degradação de pastagens e produção de bovinos de corte com a integração agricultura x pecuária. In *Simpósio de Produção de Gado de Corte*; UFV: Viçosa, Brazil, 1999; pp. 201–234.
5. Dias-Filho, M.B. *Degradação de Pastagens: Processos, Causas e Estratégias de Recuperação*, 4th ed.; Edição do Autor: Belém, PA, Brazil, 2011; 215p.
6. Bustamante, M.M.C.; Nobre, C.A.; Smeraldi, R.; Aguiar, A.P.D.; Barioni, L.G.; Ferreira, L.G.; Longo, K.; May, P.; Pinto, A.S.; Ometto, J.P.H.B. Estimating greenhouse gas emissions from cattle raising in Brazil. *Clim. Chang.* **2012**, *115*, 559–577. [CrossRef]
7. Henderson, B.B.; Gerber, P.J.; Hilinski, T.E.; Falcucci, A.; Ojima, D.S.; Salvatore, M.; Conant, R.T. Greenhouse gas mitigation potential of the world's grazing lands: Modeling soil carbon and nitrogen fluxes of mitigation practices. *Agric. Ecosyst. Environ.* **2015**, *207*, 91–100. [CrossRef]
8. Lambin, E.F.; Gibbs, H.K.; Ferreira, L.; Grau, R.; Mayaux, P.; Meyfroidt, P.; Morton, D.C.; Rudel, T.K.; Gasparri, I.; Munger, J. Estimating the world's potentially available cropland using a bottom-up approach. *Glob. Environ. Chang.* **2013**, *23*, 892–901. [CrossRef]
9. Bolfe, É.L.; Victoria, D.d.C.; Sano, E.E.; Bayma, G.; Massruhá, S.M.F.S.; de Oliveira, A.F. Potential for Agricultural Expansion in Degraded Pasture Lands in Brazil Based on Geospatial Databases. *Land* **2024**, *13*, 200. [CrossRef]
10. Fernandes, F.H.S.; Sano, E.E.; Ferreira, L.G.; Baptista, G.M.M.; de Castro Victoria, D.; Fassoni-Andrade, A.C. Degradation trends based on MODIS-derived estimates of productivity and water use efficiency: A case study for the cultivated pastures in the Brazilian Cerrado. *Remote Sens. Appl. Soc. Environ.* **2019**, *11*, 30–40. [CrossRef]
11. Pereira, O.J.R.; Ferreira, L.G.; Pinto, F.; Baumgarten, L. Assessing Pasture Degradation in the Brazilian Cerrado Based on the Analysis of MODIS NDVI Time-Series. *Remote Sens.* **2018**, *10*, 1761. [CrossRef]
12. Gosch, M.S.; Parente, L.L.; Ferreira, N.C.; Oliveira, A.R.O.; Ferreira, L.G. Pastagens degradadas, uma herança dos imóveis rurais desapropriados para os assentamentos rurais do Cerrado goiano. *Rev. Campo–Territ.* **2020**, *15*, 202–229. [CrossRef]
13. Gosch, M.S.; Parente, L.L.; dos Santos, C.O.; Mesquita, V.V.; Ferreira, L.G. Landsat-Based Assessment of the Quantitative and Qualitative Dynamics of the Pasture Areas in Rural Settlements in the Cerrado Biome, Brazil. *Appl. Geogr.* **2021**, *136*, 102585. [CrossRef]
14. Veloso, G.A.; Silva, J.R.; Ferreira, M.E.; Ferreira, L.G., Jr. Biomassa Seca Estimada Em Áreas De Pastagens Com Dados De Sensoriamento Remoto: Estudo de caso na bacia hidrográfica do Rio Vermelho-Goiás. *Soc. E Territ.* **2021**, *32*, 150–171. [CrossRef]
15. Aguiar, D.A.; Mello, M.P.; Nogueira, S.F.; Gonçalves, F.G.; Adami, M.; Rudorff, B.F.T. MODIS Time Series to Detect Anthropogenic Interventions and Degradation Processes in Tropical Pasture. *Remote Sens.* **2017**, *9*, 73. [CrossRef]
16. Baeza, S.; Paruelo, J.M. Land Use/Land Cover Change (2000–2014) in the Rio de la Plata Grasslands: An Analysis Based on MODIS NDVI Time Series. *Remote Sens.* **2020**, *12*, 381. [CrossRef]
17. Lyu, X.; Li, X.B.; Dang, D.L.; Dou, H.S.; Xuan, X.J.; Liu, S.Y.; Li, M.Y.; Gong, J.R. A new method for grassland degradation monitoring by vegetation species composition using hyperspectral remote sensing. *Ecol. Indic.* **2020**, *114*, 106310. [CrossRef]
18. Jadhav, R.N.; Kimothi, M.M.; Kandya, A.K. Grassland mapping/monitoring of Banni, Kachchh (Gujarat) using remotely-sensed data. *Int. J. Remote Sens.* **1993**, *14*, 3093–3103. [CrossRef]
19. Toivonen, T.; Luoto, M. Landsat TM images in mapping of semi-natural grasslands and analysing of habitat pattern in an agricultural landscape in south-west Finland. *Fenn. Int. J. Geogr.* **2003**, *181*, 49–67. Available online: https://fennia.journal.fi/article/view/3756 (accessed on 13 December 2023).
20. Baldi, G.; Guerschman, J.P.; Paruelo, J.M. Characterizing fragmentation in temperate South America grasslands. *Agric. Ecosyst. Environ.* **2006**, *116*, 197–208. [CrossRef]
21. Jakimov, B.; Griffiths, P.; van der Linden, S.; Hostert, P. Mapping pasture management in the Brazilian Amazon from dense Landsat time series. *Remote Sens. Environ.* **2018**, *205*, 453–468. [CrossRef]
22. Smith, A.M.; Buckley, J.R. Investigating RADARSAT-2 as a tool for monitoring grassland in western Canada. *Can. J. Remote Sens.* **2011**, *37*, 93–102. [CrossRef]

23. Darvishzadeh, R.; Atzberger, C.; Skidmore, A.; Schlerf, M. Mapping grassland leaf area index with airborne hyperspectral imagery: A comparison study of statistical approaches and inversion of radiative transfer models. *ISPRS J. Photogramm. Remote Sens.* **2011**, *66*, 894–906. [CrossRef]
24. Yang, C.; Everitt, J.H. Mapping three invasive weeds using airborne hyperspectral imagery. *Ecol. Inform.* **2010**, *5*, 429–439. [CrossRef]
25. Obermeier, W.A.; Lehnert, L.W.; Pohl, M.J.; Makowski Gianonni, S.; Silva, B.; Seibert, R.; Laser, H.; Moser, G.; Müller, C.; Luterbacher, J.; et al. Grassland ecosystem services in a changing environment: The potential of hyperspectral monitoring. *Remote Sens. Environ.* **2019**, *232*, 111273. [CrossRef]
26. Feltran-Barbieri, R.; Féres, J.G. Degraded pastures in Brazil: Improving livestock production and forest restoration. *R. Soc. Open Sci.* **2021**, *8*, 201854. [CrossRef] [PubMed]
27. Toniol, A.C.; Galvão, L.S.; Ponzoni, F.J.; Sano, E.E.; de Jesus Amore, D. Potential of hyperspectral metrics and classifiers for mapping Brazilian savannas in the rainy and dry seasons. *Remote Sens. Appl. Soc. Environ.* **2017**, *8*, 20–29. [CrossRef]
28. Jacon, A.D.; Galvão, L.S.; Dos Santos, J.R.; Sano, E.E. Seasonal characterization and discrimination of savannah physiognomies in Brazil using hyperspectral metrics from Hyperion/EO-1. *Int. J. Remote Sens.* **2017**, *38*, 4494–4516. [CrossRef]
29. Haddad, I.; Galvão, L.S.; Breunig, F.M.; Dalagnol, R.; Bourscheidt, V.; Jacon, A.D. On the combined use of phenological metrics derived from different PlanetScope vegetation indices for classifying savannas in Brazil. *Remote Sens. Appl. Soc. Environ.* **2002**, *26*, 100764. [CrossRef]
30. Araújo, J.d.A.; Galvão, L.S.; Dalagnol, R. Evaluating changes with vegetation cover in PRISMA's spectral, spatial, and temporal attributes and their performance for classifying savannahs in Brazil. *Remote Sens. Appl. Soc. Environ.* **2023**, *32*, 101074. [CrossRef]
31. Parente, L.; Taquary, E.; Silva, A.P.; Souza, C.; Ferreira, L. Next generation mapping: Combining deep learning, cloud computing, and big remote sensing data. *Remote Sens.* **2019**, *11*, 2881. [CrossRef]
32. Breiman, L. Random forests. *Mach. Learn.* **2001**, *45*, 5–32. [CrossRef]
33. Johansen, K.; Phinn, S.; Taylor, M. Mapping woody vegetation clearing in Queensland, Australia from Landsat imagery using the Google Earth Engine. *Remote Sens. Appl. Soc. Environ.* **2015**, *1*, 36–49. [CrossRef]
34. Huete, A.; Didan, K.; Miura, T.; Rodriguez, E.P.; Gao, X.; Ferreira, L.G. Overview of the radiometric and biophysical performance of the MODIS vegetation indices. *Remote Sens. Environ.* **2002**, *83*, 195–213. [CrossRef]
35. Moura, Y.M.D.; Galvão, L.S.; Hilker, T.; Wu, J.; Saleska, S.; Amaral, C.H.D.; Nelson, B.W.; Lopes, A.P.; Wiedeman, K.K.; Prohaska, N.; et al. Spectral analysis of amazon canopy phenology during the dry season using a tower hyperspectral camera and modis observations. *ISPRS J. Photogramm. Remote Sens.* **2017**, *131*, 52–64. [CrossRef]
36. Gitelson, A.A.; Kaufman, Y.J.; Merzlyak, M.N. Use of a green channel in remote sensing of global vegetation from EOS-MODIS. *Remote Sens. Environ.* **1996**, *58*, 289–298. [CrossRef]
37. Rouse, J.W.; Haas, R.H.; Schnell, J.A.; Deering, D.W. *Monitoring the Vernal Advancement and Retrogradation of Natural Vegetation*; NASA/GSFC Type II Progress Report; NASA: Greenbelt, MD, USA, 1973.
38. Gitelson, A.; Merzlyak, M.N. Spectral Reflectance Changes Associated with Autumn Senescence of *Aesculus hippocastanum* L. and *Acer platanoides* L. Leaves. Spectral Features and Relation to Chlorophyll Estimation. *J. Plant Physiol.* **1994**, *143*, 286–292. [CrossRef]
39. Galvão, L.S.; Arlanche Petri, C.; Dalagnol, R. Coupled effects of solar illumination and phenology on vegetation index determination: An analysis over the Amazonian forests using the SuperDove satellite constellation. *GISci. Remote Sens.* **2024**, *61*, 2290354. [CrossRef]
40. Teles, N.M. Sensoriamento Remoto e Escore de Condição da Pastagem para Avaliação da Qualidade e Produtividade de Pastagens. Master's Thesis, Universidade Federal de Goiás, Escola de Veterinária e Zootecnia (EVZ), Goiânia, Brazil, 2021.
41. Laboratório de Processamento de Imagens e Geoprocessamento—LAPIG. Atlas Digital das Pastagens Brasileiras. 2021. Available online: https://pastagem.org (accessed on 25 January 2024).
42. Gamon, J.; Serrano, L.; Surfus, J.S. The photochemical reflectance index: An optical indicator of photosynthetic radiation use efficiency across species, functional types, and nutrient levels. *Oecologia* **1997**, *112*, 492–501. [CrossRef] [PubMed]
43. Gruninger, J.; Ratkowski, A.; Hoke, M. The sequential maximum angle convex cone (SMACC) endmember model. *Proc. SPIE* **2004**, *5425*, 1–14. [CrossRef]
44. Roberts, D.A.; Smith, M.O.; Adams, J.B. Green vegetation, nonphotosynthetic vegetation, and soils in AVIRIS data. *Remote Sens. Environ.* **1993**, *44*, 255–269. [CrossRef]
45. Van der Meer, F. Analysis of spectral absorption features in hyperspectral imagery. *Int. J. Appl. Earth Obs. Geoinf.* **2004**, *5*, 55–68. [CrossRef]
46. Haralick, R.; Shanmugam, K.; Dinstein, I. Textural features for image classification. *IEEE Trans. Syst. Man Cybern.* **1973**, *6*, 610–621. [CrossRef]
47. Wood, E.M.; Pidgeon, A.M.; Radeloff, V.C.; Keuler, N.S. Image texture as a remotely sensed measure of vegetation structure. *Remote Sens. Environ.* **2012**, *121*, 516–526. [CrossRef]
48. Zhou, W.; Yang, H.; Huang, L.; Chen, C.; Lin, X.S.; Hu, Z.J.; Li, J.L. Grassland degradation remote sensing monitoring and driving factors quantitative assessment in China from 1982 to 2010. *Ecol. Indic.* **2017**, *83*, 303–313. [CrossRef]

49. Sano, E.E.; Bezerra, H.D.S.; Barcellos, A.D.O.; Rosa, R. Metodologias para Mapeamento de Pastagens Degradadas no Cerrado. In *Boletim de Pesquisa e Desenvolvimento*; Embrapa: Brasília, Brazil, 2002; pp. 1–22. Available online: https://ainfo.cnptia.embrapa.br/digital/bitstream/CPAC-2009/24654/1/bolpd_70.pdf (accessed on 15 January 2024).
50. Jacon, A.D.; Galvão, L.S.; Dalagnol, R.; Dos Santos, J.R. Aboveground biomass estimates over Brazilian savannas using hyperspectral metrics and machine learning models: Experiences with Hyperion/EO-1. *Gisci. Remote Sens.* **2021**, *58*, 112–1129. [CrossRef]
51. De Torres, F.N.; Richter, R.; Vohland, M. A multisensoral approach for high-resolution land cover and pasture degradation mapping in the humid tropics: A case study of the fragmented landscape of Rio de Janeiro. *Int. J. Appl. Earth Obs. Geoinf.* **2019**, *78*, 189–201. [CrossRef]
52. Karnieli, A.; Bayarjargal, Y.; Bayasgalan, M.; Mandakh, B.; Dugarjav, C.; Burgheimer, J.; Khudulmur, S.; Bazha, S.N.; Gunin, P.D. Do vegetation indices provide a reliable indication of vegetation degradation? A case study in the Mongolian pastures. *Int. J. Remote Sens.* **2013**, *34*, 6243–6262. [CrossRef]
53. Sano, E.E.; Bolfe, É.L.; Parreiras, T.C.; Bettiol, G.M.; Vicente, L.E.; Sanches, I.D.; Victoria, D.d.C. Estimating Double Cropping Plantations in the Brazilian Cerrado through PlanetScope Monthly Mosaics. *Land* **2023**, *12*, 581. [CrossRef]

Disclaimer/Publisher's Note: The statements, opinions and data contained in all publications are solely those of the individual author(s) and contributor(s) and not of MDPI and/or the editor(s). MDPI and/or the editor(s) disclaim responsibility for any injury to people or property resulting from any ideas, methods, instructions or products referred to in the content.